27. Jennings, B., Preiss, A., Delidakis, C. & Bray, S. The Notch signalling pathway is required for *Enhancer of split* bHLH protein expression during neurogenesis in the *Drosophila* embryo. *Development* **120**, 3537–3548 (1994).

28. Wesley, C. S. & Saez, L. Analysis of Notch lacking the carboxyl terminus identified in *Drosophila* embryos. *J. Cell. Biol.* **149**, 683–696 (2000).

29. Blaumueller, C. M. et al. Intracellular cleavage of Notch leads to a heterodimeric receptor on the plasma membrane. *Cell* **90**, 281–291 (1997).

....

Polarity controls forces governing asymmetric spindle positioning in the *Caenorhabditis elegans* embryo

Stephan W. Grill*†, **Pierre Gönczy***‡, **Ernst H. K. Stelzer*** & **Anthony A. Hyman**†

* *European Molecular Biology Laboratory (EMBL), D-69117 Heidelberg, Germany*
† *Max-Planck-Institute for Cell Biology and Genetics (MPI-CBG), D-01307 Dresden, Germany*

....

Cell divisions that create daughter cells of different sizes are crucial for the generation of cell diversity during animal development[1]. In such asymmetric divisions, the mitotic spindle must be asymmetrically positioned at the end of anaphase[2,3]. The mechanisms by which cell polarity translates to asymmetric spindle positioning remain unclear. Here we examine the nature of the forces governing asymmetric spindle positioning in the single-cell-stage *Caenorhabditis elegans* embryo. To reveal the forces that act on each spindle pole, we removed the central spindle in living embryos either physically with an ultraviolet laser microbeam, or genetically by RNA-mediated interference of a kinesin[4]. We show that pulling forces external to the spindle act on the two spindle poles. A stronger net force acts on the posterior pole, thereby explaining the overall posterior displacement seen in wild-type embryos. We also show that the net force acting on each spindle pole is under control of the *par* genes that are required for cell polarity along the anterior–posterior embryonic axis. Finally, we discuss simple mathematical models that describe the main features of spindle pole behaviour. Our work suggests a mechanism for generating asymmetry in spindle positioning by varying the net pulling force that acts on each spindle pole, thus allowing for the generation of daughter cells with different sizes.

The first cleavage division of *C. elegans* embryos generates a large anterior and a smaller posterior blastomere along the anterior–posterior axis[5]. Polarity in this system is established after fertilization[6] by the concerted action of at least six *par* genes[7]. During anaphase B, the spindle elongates asymmetrically: the anterior spindle pole remains in a relatively fixed position along the anterior–posterior axis, while the posterior spindle pole is displaced towards the posterior of the embryo as it oscillates transversely[8].

Two types of microtubule-dependent forces contribute to spindle positioning and elongation during anaphase B in other systems[9–12]. First, overlapping spindle microtubules can generate forces that 'push' spindle poles apart[9]. Second, forces transmitted by astral microtubules can 'pull' spindle poles apart[10–12]. To test which of these apply to the one-cell *C. elegans* embryo, we removed the spindle midzone that connects the two spindle poles at the beginning of anaphase B, and examined the resulting movement of the two independent spindle poles. If intra-spindle forces alone drive anaphase B, then the two spindle poles should not separate after the spindle is severed. In contrast, if extra-spindle pulling forces participate in anaphase B, separation of the two spindle poles should still occur after severing. The spindle midzone was severed with a pulsed ultraviolet laser microbeam, or removed by RNA mediated interference (RNAi)[4] of a *C. elegans* kinesin that is related to XKCM1/MCAK[13–16] (referred to as CeMCAK). In both experimental situations, we verified the disappearance of the spindle midzone by immunofluorescence with anti-tubulin antibodies (Fig. 1b, c; compare with Fig. 1a, arrows). The effect was spatially confined, as astral microtubules were not affected (Fig. 1b, c; compare with Fig. 1a, arrowheads).

We tracked each spindle pole using time-lapse differential interference contrast (DIC) microscopy. This showed both a dramatic increase in pole to pole distance (Fig. 2b, c; compare with Fig. 2a, arrowheads) and an increase in peak velocities of the spindle poles (Fig. 3) after removal of the spindle. Together, these results demonstrate that forces external to the spindle act on the spindle poles during anaphase B. Notably, in both of the experimental situations, the posterior spindle pole behaved differently compared with the anterior one (Figs 2 and 3). The posterior pole covered a greater distance, travelled at about a 40% higher peak velocity, and underwent transverse oscillations in the proximity of the cell cortex. This suggests that a greater pull acts on the posterior spindle pole than on its anterior counterpart, which may explain the overall posterior displacement of the spindle during anaphase B in wild-type embryos. Formally, a change in viscous drag could account for the observed differences in peak velocities, although this is unlikely, on the basis of an analysis of yolk-granule motion (see Methods).

We next examined how the *par* genes influence the net pulling
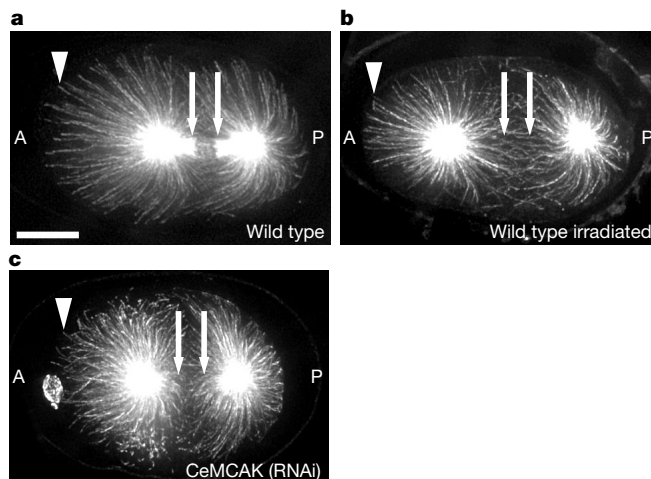
Figure 1 Spindle midzone viewed by indirect immunofluorescence with anti-tubulin antibodies. All embryos are in anaphase B. Anterior (A) is on the left and posterior (P) is on the right in this and all other figures. Scale bar, 10 μm. **a**, In wild-type embryos, both the spindle microtubules (arrows) and astral microtubules (arrowheads) are visible. **b**, **c**, Both in the wild-type irradiated and in the CeMCAK (RNAi) embryos astral microtubules are visible (arrowheads), but spindle microtubules are not (arrows).

force that acts on each spindle pole. We focused on *par-2* and *par-3*. In embryos that are mutant for either of the genes, the spindle is symmetrically positioned throughout anaphase B, presumably as a consequence of defects in establishing polarity along the anterior–posterior axis[17]. In wild-type embryos, PAR-3 is restricted to the anterior cortex[18], and PAR-2 to the posterior cortex[19]. In *par-2* mutants, PAR-3 is found both at the posterior and anterior cortex of the embryo, which leads to a cortex that has anterior character throughout[7,18,20]. Conversely, in *par-3* mutant embryos, PAR-2 fills the entire cortex of the embryo, which subsequently has posterior character throughout[19,20].

Our spindle-severing experiments in the wild-type embryo predict that in a *par-2* mutant embryo, the pull acting on both of the spindle poles should be equal, and resemble that exerted on the anterior spindle pole of wild-type embryos. In a *par-3* mutant embryo, the pull acting on both of the spindle poles should be equal, and resemble that exerted on the posterior spindle pole of wild-type embryos. We tested these predictions by severing the spindle midzone with an ultraviolet laser microbeam. Strikingly, in severed *par-2* mutant embryos, the resulting peak velocities of both spindle poles resembled that of the anterior spindle pole in wild-type irradiated embryos (Fig. 3). Conversely, in severed *par-3* mutant embryos, peak velocities of both spindle poles resembled that of the

posterior spindle pole in wild-type irradiated embryos (Fig. 3). Furthermore, spindle breakage events still occurred when both PAR-3 and CeMCAK were removed, whereas none were observed when the expression of both *par-2* and CeMCAK was abolished by RNAi (see Supplementary Information). This indicates that the net forces acting on both of the spindle poles in the absence of *par-2* function are not strong enough to trigger spindle rupture. All these observations show that the first division in *par-2* and *par-3* mutant embryos is symmetric because of distinct alterations in forces pulling on the spindle poles, both of which lead to equally strong pulling forces being exerted on either side.

We have shown that polarity translates into asymmetric spindle positioning by modulating the net pulling force that acts on each spindle pole; in wild-type embryos, the net pull on the posterior pole is more extensive, which leads to a displacement of the spindle towards the posterior. Force generation may be actin-dependent, although this is unlikely, as disruption of actin filaments by cytochalasin during anaphase B does not affect spindle positioning[21]. Pulling forces are more likely to be mediated by astral microtubules[11], perhaps by coupling force generation to microtubule depolymerization at the cell cortex[22–24]. How the PAR proteins modulate cytoskeletal behaviour to control the net pulling force that acts on each spindle pole remains unknown. Any model
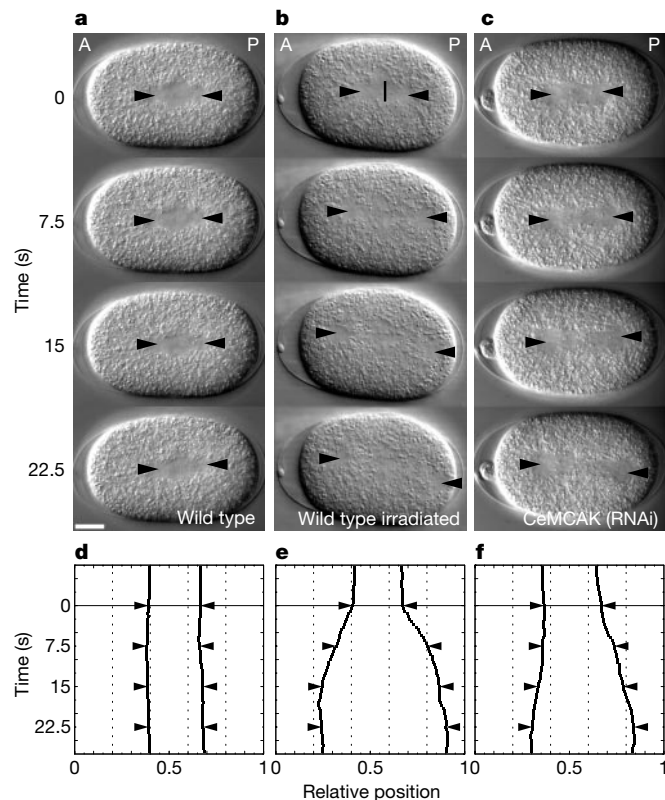
Figure 2 Pole-to-pole distance increases after spindle severing. **a**–**c**, Differential interference contrast (DIC) image series of *C. elegans* embryos. Spindle poles are indicated (arrowheads). Scale bar, 10 μm. **a**, Wild-type embryo. **b**, Irradiated wild-type embryo. The bar indicates where the spindle was destroyed. **c**, CeMCAK (RNAi) embryo. Spindle breakage takes place at 0 s. For both **b** and **c**, the posterior spindle pole travels further and faster than the anterior one, and a slight transverse displacement is seen in the last frame, corresponding to the beginning of transverse oscillations. Removal of ZEN-4 also results in diminished midzone microtubules without affecting anaphase B movements[29,30]. However, the timing of spindle breakage seems to be different, leading to a more subtle effect on spindle-pole velocity during anaphase (see Supplementary Information). **d**–**f**, Corresponding traces of relative spindle-pole position along the anterior–posterior axis, arrowheads indicate time points for which frames in **a**–**c** are displayed.
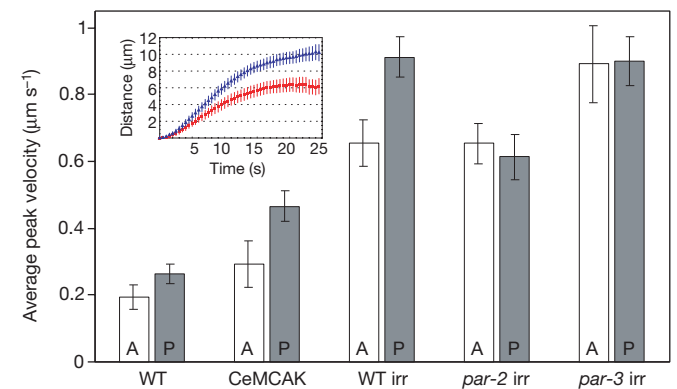
Figure 3 Average peak velocities of spindle poles increase after spindle severing. All error columns are s.e.m. with a confidence interval of 0.95. Bars show the average peak velocities of spindle poles along the anterior–posterior axis. White and black bars indicate the anterior and posterior spindle pole, respectively. Average peak velocities of spindle poles during anaphase B in wild-type (WT, *n* = 20), CeMCAK (RNAi) (CeMCAK, *n* = 20), wild-type irradiated (WT irr, *n* = 34), *par-2* (*it5*) irradiated (*par-2* irr, *n* = 30) and *par-3* (*it71*) irradiated embryos (*par-3* irr, *n* = 20) are shown. Inset, average displacement of anterior spindle pole (red) and posterior spindle pole (blue) after irradiation in wild-type embryos (*n* = 34); actual movements are in opposite directions.
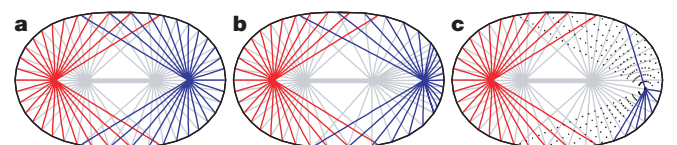
Figure 4 Numerical simulation of spindle-pole behaviour after spindle severing. The anterior aster (red) and posterior aster (blue) are shown. Grey indicates the initial state just before severing. Colours indicate the state after 22.5 s. **a**, The posterior microtubules all exert a greater pulling force than the anterior ones. **b**, All microtubules generate the same force, but the density of microtubules is increased at the very posterior end. **c**, All microtubules generate the same pulling force, but the cortical connection is weak for all microtubules of the posterior aster: they detach from the cortex instead of getting longer. Dashed lines indicate microtubules that are inactive for 12 s. Only **c** reproduces the experimental behaviour, as the posterior spindle pole travels further and faster than the anterior one, and undergoes transverse oscillations (compare with Fig. 2b and c).

describing net force generation must account for three features of spindle-pole behaviour after spindle severing (see Figs 2 and 3): the posterior spindle pole travels further than the anterior one, it travels faster, and it undergoes transverse oscillations in the proximity of the cell cortex. One possible mechanism may be that all microtubules of the posterior aster generate pulling forces that are stronger than that of the anterior aster. However, numerical simulations of this model only satisfy one of the three features, that being the posterior spindle pole travelling faster than the anterior one (Fig. 4a; see also Methods and Supplementary Information). A different hypothesis invokes an increase of forces for a subset of microtubules of the posterior aster or, similarly, an increase of microtubule density in a specific region at the posterior. Numerical simulations of this model show faster movement and a greater distance travelled by the posterior pole (Fig. 4b and Methods), but no transverse oscillations. A simpler hypothesis is that all microtubules of both asters generate equal forces, but that the interactions between microtubules and the posterior cortex are weaker than those of the anterior cortex. As an example, if microtubules of the posterior aster were to detach from the cortex instead of elongating, the net force would increase in the direction of movement. Numerical simulations of this model satisfy all three features (Fig. 4c; see also Methods).

Notably, PAR-3 has been proposed to anchor or stabilize microtubules[18,20,25], and it is absent from the posterior cortex, suggesting a possible mechanism for differential microtubule stability. Although the underlying molecular nature remains to be determined, our model suggests a plausible mechanism of how polarity controls cytoskeletal behaviour to ultimately generate two daughter cells of different sizes. □

Methods

Culture conditions, strains and time-lapse recordings

Basic methods of *C. elegans* culture and handling were used as described[26]. We used strains carrying the following mutations: *daf-7* (*e1372*) *par-2* (*it5*) III (ref. 17) and *par-3* (*it71*) *unc-32* (*e189*)/qC1 (refs 20, 27). Embryos that were derived from homozygous mutant mothers are referred to as mutant embryos. We grew wild-type and *par-3* nematodes at 16 °C. *par-2* nematodes were grown at 16 °C until L3, and then shifted to 25 °C. We followed standard procedures for sample preparation and time-lapse DIC recordings at two frames per second[28]. Polarity of the embryos was determined in all cases by examining the position of the male pronucleus, which defines the posterior of the embryo[6].

Spindle severing

Experiments were performed using an ultraviolet laser microdissection apparatus (P.A.L.M. Mikrolaser Technologie GmbH). We focused the pulsed N_2 laser ($\lambda = 337$ nm) to a ~3-μm spot in the focal plane. *C. elegans* embryos were mounted on the inverted microscope, and as soon as a slight transverse movement of the posterior spindle pole became visible (indicating the beginning of anaphase B) about 10 shots at 30 Hz were taken at the spindle midzone. If the same number of shots were taken at regions between the spindle and the cell cortex, an increase of pole-to-pole distance was not observed (data not shown). All experimental results were verified by irradiating either the posterior or the anterior spindle pole and observing the behaviour of the other spindle pole respectively (data not shown).

RNAi of the *C. elegans* kinesin CeMCAK

We performed RNAi of the kinesin CeMCAK (gene K11D9.1) using standard procedures[16], and using the primers 5′-AATTAACCCTCACTAAAGGTCCTGTTCGTAT GGCTCCTC-3′ and 5′-TAATACGACTCACTATAGGTCCTCTTTGAGCCCAACAAC-3′.

Single-embryo indirect immunofluorescence

Indirect immunofluorescence of single embryos was carried out with some modifications to allow for visualizing single embryos at defined stages. One pronuclear-migration-stage embryo was pipetted on a 24 × 60 mm² coverslip that was previously coated with 1% poly-L-lysine (Sigma, P1524) in PBS. The embryo was imaged on the inverted microscope, the spindle midzone was irradiated (when applicable) and the embryo then fixed by a 'freeze-crack' procedure as described[28]. We followed standard methods[28] for antibody staining. Images were recorded using a widefield DeltaVision microscope (Applied Precision) and deconvolved. Figure 1 shows 2-μm projections.

Data acquisition and analysis

The positions of both of the spindle poles were manually tracked in the DIC recordings.

We smoothed tracking data using an eight-frame running average filter, as this gave consistent results for repeated tracking of movies.

Analysis of yolk-granule motion

The observed difference in peak velocities of the anterior in comparison to the posterior spindle pole after spindle severing may be attributed to a change in viscous drag. As yolk granules probably have a large function in hindering spindle-pole movement, a mean square displacement (MSD) analysis was performed for 182 yolk granules located close to the anterior or the posterior cell cortex. Granules were automatically tracked every 0.5 s for a duration of 25 s. On a 5-s timescale, MSD plots were characteristic for either normal diffusion or for simultaneous diffusion and flow. We determined diffusion coefficients for the normal diffusing granules; their average diffusion coefficient at the anterior was less than 6% higher than their average diffusion coefficient at the posterior (data not shown). As diffusive properties of granules at the anterior versus the posterior are alike, and because spindle-pole structures are of similar size (Fig. 1a), it is unlikely that a ~40% difference in peak velocities only results from a difference in viscous drag.

Spindle-pole behaviour after spindle severing

In these descriptive two-dimensional models of spindle-pole behaviour, we assume that forces driving spindle-pole movement after severing are mediated by astral microtubules. We also assume that astral microtubules connect to a fixed position on the cell cortex (see Fig. 1a, arrowhead), and that they exert an equal pulling force on the spindle pole in the direction of the cortical connection. The evidence that microtubules are exerting pulling forces comes from experiments where regions between the spindle pole and the cell cortex are irradiated, which results in displacement of the spindle pole towards the opposite cell cortex (data not shown). The simulation is carried out by iteratively performing three steps. First, the net force acting on each spindle pole is calculated by summing up the contributing forces of the 25 individual microtubules. Second, the spindle pole is displaced proportionally to the net force, consistent with movement in a completely damped, viscous regime. Third (Fig. 4c only), microtubules that have increased length as a result of spindle-pole displacement are inactivated for a latency time of 12 s.

1. Horvitz, H. R. & Herskowitz, I. Mechanisms of asymmetric cell division: two Bs or not two Bs, that is the question. *Cell* **68**, 237–255 (1992).
2. Rappaport, R. Cytokinesis in animal cells. *Int. Rev. Cytol.* **31**, 169–213 (1971).
3. Gönczy, P. & Hyman, A. A. Cortical domains and the mechanisms of asymmetric cell division. *Trends Cell Biol.* **6**, 382–387 (1996).
4. Fire, A. *et al.* Potent and specific genetic interference by double-stranded RNA in *Caenorhabditis elegans*. *Nature* **391**, 806–811 (1998).
5. Sulston, J. E., Schierenberg, E., White, J. G. & Thomson, J. N. The embryonic cell lineage of the nematode *Caenorhabditis elegans*. *Dev. Biol.* **100**, 64–119 (1983).
6. Goldstein, B. & Hird, S. N. Specification of the anteroposterior axis in *Caenorhabditis elegans*. *Development* **122**, 1467–1474 (1996).
7. Kemphues, K. J. & Strome, S. in *C. elegans II* (eds Riddle, D. L., Blumenthal, T., Meyer, B. J. & Priess, J. R.) 335–359 (Cold Spring Harbor Laboratory, New York, 1997).
8. Albertson, D. Formation of the first cleavage spindle in nematode embryos. *Dev. Biol.* **101**, 61–72 (1984).
9. Leslie, R. J. & Pickett, H. J. Ultraviolet microbeam irradiations of mitotic diatoms: investigation of spindle elongation. *J. Cell Biol.* **96**, 548–561 (1983).
10. Aist, J. R. & Berns, M. W. Mechanics of chromosome separation during mitosis in *Fusarium* (Fungi imperfecti): new evidence from laser microbeam experiments. *J. Cell Biol.* **91**, 446–458 (1981).
11. Aist, J. R., Liang, H. & Berns, M. W. Astral and spindle forces in PtK2 cells during anaphase B: a laser microbeam study. *J. Cell Sci.* **104**, 1207–1216 (1993).
12. Waters, J. C., Cole, R. W. & Rieder, C. L. The force-producing mechanism for centrosome separation during spindle formation in vertebrates is intrinsic to each aster. *J. Cell Biol.* **122**, 361–372 (1993).
13. Wordeman, L. & Mitchison, T. J. Identification and partial characterization of mitotic centromere-associated kinesin, a kinesin-related protein that associates with centromeres during mitosis. *J. Cell Biol.* **128**, 95–104 (1995).
14. Wein, H., Foss, M., Brady, B. & Cande, W. Z. DSK1, a novel kinesin-related protein from the diatom *Cylindrotheca fusiformis* that is involved in anaphase spindle elongation. *J. Cell Biol.* **133**, 595–604 (1996).
15. Desai, A., Verma, S., Mitchison, T. J. & Walczak, C. E. Kin I kinesins are microtubule-destabilizing enzymes. *Cell* **96**, 69–78 (1999).
16. Gönczy, P. *et al.* Functional genomic analysis of cell division in *C. elegans* using RNAi of genes on chromosome III. *Nature* **408**, 331–336 (2000).
17. Kemphues, K. J., Priess, J. R., Morton, D. G. & Cheng, N. Identification of genes required for cytoplasmic localization in early *C. elegans* embryos. *Cell* **52**, 311–320 (1988).
18. Etemad-Moghadam, B., Guo, S. & Kemphues, K. J. Asymmetrically distributed PAR-3 protein contributes to cell polarity and spindle alignment in early *C. elegans* embryos. *Cell* **83**, 743–752 (1995).
19. Boyd, L., Guo, S., Levitan, D., Stinchcomb, D. T. & Kemphues, K. J. PAR-2 is asymmetrically distributed and promotes association of P granules and PAR-1 with the cortex in *C. elegans* embryos. *Development* **122**, 3075–3084 (1995).
20. Cheng, N. N., Kirby, C. M. & Kemphues, K. J. Control of cleavage spindle orientation in *Caenorhabditis elegans*: the role of the genes par-2 and par-3. *Genetics* **139**, 549–559 (1995).
21. Hill, D. P. & Strome, S. An analysis of the role of microfilaments in the establishment and maintenance of asymmetry in *Caenorhabditis elegans* zygotes. *Dev. Biol.* **125**, 75–84 (1988).
22. Hyman, A. A. & White, J. G. Determination of cell division axes in the early embryogenesis of *Caenorhabditis elegans*. *J. Cell Biol.* **105**, 2123–2135 (1987).

23. Lee, L. *et al.* Positioning of the mitotic spindle by a cortical-microtubule capture mechanism. *Science* **287,** 2260–2262 (2000).
24. Korinek, W. S., Copeland, M. J., Chaudhuri, A. & Chant, J. Molecular linkage underlying microtubule orientation toward cortical sites in Yeast. *Science* **287,** 2257–2259 (2000).
25. Rose, L. S. & Kemphues, K. The let-99 gene is required for proper spindle orientation during cleavage of the *C. elegans* embryo. *Development* **125,** 1337–1346 (1998).
26. Brenner, S. The genetics of *Caenorhabditis elegans. Genetics* **77,** 71–94 (1974).
27. Morton, D. G., Roos, J. M. & Kemphues, K. J. *par-4*, a gene required for cytoplasmic localisation and determination of specific cell types in *Caenorhabditis elegans* embryogenesis. *Genetics* **130,** 771–790 (1992).
28. Gönczy, P. *et al.* Dissection of cell division processes in the one cell stage *Caenorhabditis elegans* embryo by mutational analysis. *J. Cell Biol.* **144,** 927–946 (1999).
29. Raich, W. B., Moran, A. N., Rothman, J. H. & Hardin, J. Cytokinesis and midzone microtubule organization in *Caenorhabditis elegans* require the kinesin-like protein ZEN-4. *Mol. Biol. Cell* **9,** 2037–2049 (1998).
30. Powers, J., Bossinger, O., Rose, D., Strome, S. & Saxton, W. A nematode kinesin required for cleavage furrow advancement. *Curr. Biol.* **8,** 1133–1136 (1998).

....

Normal human mammary epithelial cells spontaneously escape senescence and acquire genomic changes

Serguei R. Romanov*, **B. Krystyna Kozakiewicz***, **Charles R. Holst***, **Martha R. Stampfer**†, **Larisa M. Haupt*** & **Thea D. Tlsty***

* *Department of Pathology and UCSF Comprehensive Cancer Center, University of California at San Francisco, San Francisco, California 94143-0506, USA*
† *Lawrence Berkeley National Laboratory, Berkeley, California 94720, USA*

....

Senescence and genomic integrity are thought to be important barriers in the development of malignant lesions[1]. Human fibroblasts undergo a limited number of cell divisions before entering an irreversible arrest, called senescence[2]. Here we show that human mammary epithelial cells (HMECs) do not conform to this paradigm of senescence. In contrast to fibroblasts, HMECs exhibit an initial growth phase that is followed by a transient growth plateau (termed selection or M0; refs 3–5), from which proliferative cells emerge to undergo further population doublings (∼20–70), before entering a second growth plateau (previously termed senescence or M1; refs 4–6). We find that the first growth plateau exhibits characteristics of senescence but is not an insurmountable barrier to further growth. HMECs emerge from senescence, exhibit eroding telomeric sequences and ultimately enter telomere-based crisis to generate the types of chromosomal abnormalities seen in the earliest lesions of breast cancer. Growth past senescent barriers may be a pivotal event in the earliest steps of carcinogenesis, providing many genetic changes that predicate oncogenic evolution. The differences between epithelial cells and fibroblasts provide new insights into the mechanistic basis of neoplastic transformation.

To analyse cell-specific differences in growth and senescence, we characterized the *in vitro* proliferation barriers in isogenic HMECs and human mammary fibroblasts (HMFs) from healthy individuals[3,7,8]. Similar to previous studies in human skin fibroblasts[1] and HMECs[3–5,9], both the epithelial and fibroblast cell populations underwent a limited number of population doublings before entering a plateau (Fig. 1, HMF phase b, HMEC phase b). This plateau in fibroblasts has been variously termed the Hayflick limit[2], irreversible replicative senescence, and mortality stage 1 (M1)[1]). The cells enlarged in size, flattened in shape, became vacuolated (Fig. 1), and expressed senescence-associated β-galactosidase[10] (SA-β-gal; data not shown).

Low incorporation of bromodeoxyuridine (BrdU) and minimal presence of MCM2 protein, a DNA replication licensing factor[26], indicated a low proliferative index. In addition, Annexin-V staining indicated a low death index (data not shown). Further characterization showed that human foreskin fibroblasts, pre-selection HMECs and HMFs each (1) maintained genomic integrity (Fig. 2; ref. 8); (2) maintained intact cell-cycle checkpoint control (data not shown); (3) exhibited a 2N to 4N DNA content ratio of ≈ 4 at phase b (Table 1); and (4) had mean telomere restriction fragment (TRF) lengths that were similar at senescence (Fig. 3). By the morphological, behavioural and molecular criteria described above, HMFs and HMECs senesce in a manner similar to human skin fibroblasts[1]. 'M0' of HMECs thus corresponds to 'M1' of fibroblasts.

The ability of HMECs and HMFs to spontaneously overcome senescence differs by several orders of magnitude. In skin fibroblasts, senescence can last for years (at least 3 yr; T.D.T., unpublished data), cells remain viable if fed routinely[11], and the frequency of
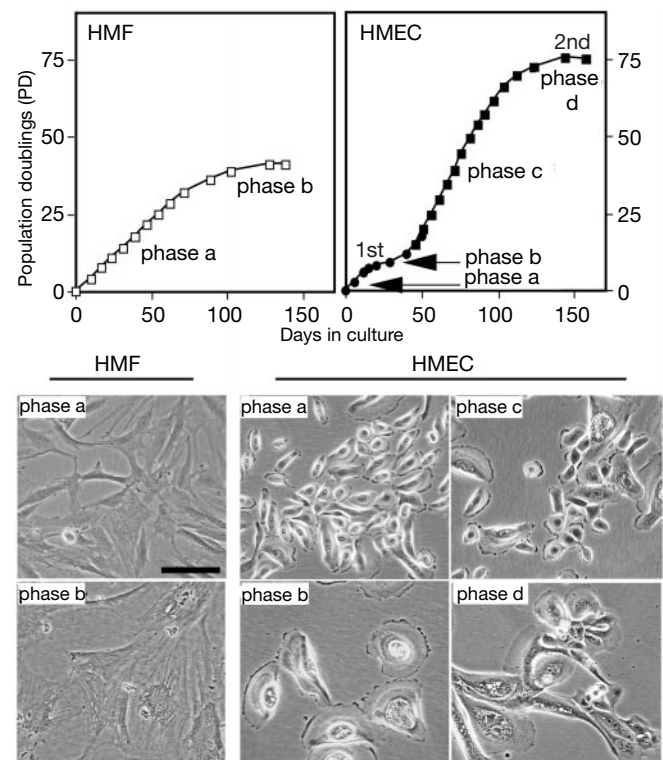
Figure 1 HMF and HMEC growth curves and cell morphologies *in vitro*. Tissue was dissociated with collagenase and hyaluronidase, and plated in parallel cultures: one in medium (DMEM) that supported the growth of fibroblasts and the other in medium (MEGM) that supported the growth of epithelial cells. The growth curve and microscopic morphology of both mammary fibroblast and epithelial cells from donor 48 during the first phase of logarithmic growth (phase a), and the first growth plateau (phase b) are shown for each population. The second epithelial phase of proliferation (phase c) and the second epithelial growth plateau (phase d) are also shown. Scale bar, 100 μm.